CLNS 06/1956
CLEO 06-05

Measurement of Interfering $K^{*+}K^-$ and $K^{*-}K^+$ Amplitudes in the Decay $D^0 \to K^+K^-\pi^0$

C. Cawlfield,[1] B. I. Eisenstein,[1] I. Karliner,[1] D. Kim,[1] N. Lowrey,[1] P. Naik,[1] C. Sedlack,[1] M. Selen,[1] E. J. White,[1] J. Wiss,[1] M. R. Shepherd,[2] D. Besson,[3] T. K. Pedlar,[4] D. Cronin-Hennessy,[5] K. Y. Gao,[5] D. T. Gong,[5] J. Hietala,[5] Y. Kubota,[5] T. Klein,[5] B. W. Lang,[5] R. Poling,[5] A. W. Scott,[5] A. Smith,[5] S. Dobbs,[6] Z. Metreveli,[6] K. K. Seth,[6] A. Tomaradze,[6] P. Zweber,[6] J. Ernst,[7] H. Severini,[8] S. A. Dytman,[9] W. Love,[9] V. Savinov,[9] O. Aquines,[10] Z. Li,[10] A. Lopez,[10] S. Mehrabyan,[10] H. Mendez,[10] J. Ramirez,[10] G. S. Huang,[11] D. H. Miller,[11] V. Pavlunin,[11] B. Sanghi,[11] I. P. J. Shipsey,[11] B. Xin,[11] G. S. Adams,[12] M. Anderson,[12] J. P. Cummings,[12] I. Danko,[12] J. Napolitano,[12] Q. He,[13] J. Insler,[13] H. Muramatsu,[13] C. S. Park,[13] E. H. Thorndike,[13] T. E. Coan,[14] Y. S. Gao,[14] F. Liu,[14] M. Artuso,[15] S. Blusk,[15] J. Butt,[15] J. Li,[15] N. Menaa,[15] R. Mountain,[15] S. Nisar,[15] K. Randrianarivony,[15] R. Redjimi,[15] R. Sia,[15] T. Skwarnicki,[15] S. Stone,[15] J. C. Wang,[15] K. Zhang,[15] S. E. Csorna,[16] G. Bonvicini,[17] D. Cinabro,[17] M. Dubrovin,[17] A. Lincoln,[17] D. M. Asner,[18] K. W. Edwards,[18] R. A. Briere,[19] J. Chen,[19] T. Ferguson,[19] G. Tatishvili,[19] H. Vogel,[19] M. E. Watkins,[19] J. L. Rosner,[20] N. E. Adam,[21] J. P. Alexander,[21] K. Berkelman,[21] D. G. Cassel,[21] J. E. Duboscq,[21] K. M. Ecklund,[21] R. Ehrlich,[21] L. Fields,[21] L. Gibbons,[21] R. Gray,[21] S. W. Gray,[21] D. L. Hartill,[21] B. K. Heltsley,[21] D. Hertz,[21] C. D. Jones,[21] J. Kandaswamy,[21] D. L. Kreinick,[21] V. E. Kuznetsov,[21] H. Mahlke-Krüger,[21] T. O. Meyer,[21] P. U. E. Onyisi,[21] J. R. Patterson,[21] D. Peterson,[21] J. Pivarski,[21] D. Riley,[21] A. Ryd,[21] A. J. Sadoff,[21] H. Schwarthoff,[21] X. Shi,[21] S. Stroiney,[21] W. M. Sun,[21] T. Wilksen,[21] M. Weinberger,[21] S. B. Athar,[22] R. Patel,[22] V. Potlia,[22] H. Stoeck,[22] J. Yelton,[22] and P. Rubin[23]

(CLEO Collaboration)

[1] *University of Illinois, Urbana-Champaign, Illinois 61801*
[2] *Indiana University, Bloomington, Indiana 47405*
[3] *University of Kansas, Lawrence, Kansas 66045*
[4] *Luther College, Decorah, Iowa 52101*
[5] *University of Minnesota, Minneapolis, Minnesota 55455*
[6] *Northwestern University, Evanston, Illinois 60208*
[7] *State University of New York at Albany, Albany, New York 12222*
[8] *University of Oklahoma, Norman, Oklahoma 73019*
[9] *University of Pittsburgh, Pittsburgh, Pennsylvania 15260*
[10] *University of Puerto Rico, Mayaguez, Puerto Rico 00681*
[11] *Purdue University, West Lafayette, Indiana 47907*
[12] *Rensselaer Polytechnic Institute, Troy, New York 12180*
[13] *University of Rochester, Rochester, New York 14627*
[14] *Southern Methodist University, Dallas, Texas 75275*
[15] *Syracuse University, Syracuse, New York 13244*
[16] *Vanderbilt University, Nashville, Tennessee 37235*
[17] *Wayne State University, Detroit, Michigan 48202*
[18] *Carleton University, Ottawa, Ontario, Canada K1S 5B6*
[19] *Carnegie Mellon University, Pittsburgh, Pennsylvania 15213*

[20]*Enrico Fermi Institute, University of Chicago, Chicago, Illinois 60637*
[21]*Cornell University, Ithaca, New York 14853*
[22]*University of Florida, Gainesville, Florida 32611*
[23]*George Mason University, Fairfax, Virginia 22030*
(Dated: June 14, 2006)

Abstract

We have studied the Cabibbo-suppressed decay mode $D^0 \to K^+K^-\pi^0$ using a Dalitz plot technique and find the strong phase difference $\delta_D \equiv \delta_{K^{*-}K^+} - \delta_{K^{*+}K^-} = 332^\circ \pm 8^\circ \pm 11^\circ$ and relative amplitude $r_D \equiv a_{K^{*-}K^+} \ / \ a_{K^{*+}K^-} = 0.52 \pm 0.05 \pm 0.04$. This measurement indicates significant destructive interference between $D^0 \to K^+(K^-\pi^0)_{K^{*-}}$ and $D^0 \to K^-(K^+\pi^0)_{K^{*+}}$ in the Dalitz plot region where these two modes overlap. This analysis uses 9.0 fb^{-1} of data collected at $\sqrt{s} \approx 10.58$ GeV with the CLEO III detector.

The determination of the Cabibbo-Kobayashi-Maskawa (CKM) angle γ (also referred to as ϕ_3) is important, yet challenging. Currently γ is inferred to be $58.6^{\circ}{}^{+6.8^{\circ}}_{-5.9^{\circ}}$ from various experimental and theoretical constraints [1]. Grossman, Ligeti, and Soffer [2] have proposed a method for a direct measurement of γ by studying $B^{\pm} \to DK^{\pm}$, where the neutral D meson ($D^0/\overline{D}^0$) decays to $K^{*+}K^-$ or $K^{*-}K^+$. An important ingredient in this analysis is the knowledge of the relative complex amplitudes of $\overline{D}^0 \to K^{*+}K^-$ and $D^0 \to K^{*+}K^-$, which, in the absence of CP violation, is the same as that between $D^0 \to K^{*-}K^+$ and $D^0 \to K^{*+}K^-$. The main goal of the analysis described here is to measure the strong phase difference δ_D and relative amplitude r_D between $D^0 \to K^{*-}K^+$ and $D^0 \to K^{*+}K^-$, which is required for the proposed extraction of γ. We are further motivated by a recent paper of Rosner and Suprun [3] that points out the sensitivity to δ_D using $D^0 \to K^+K^-\pi^0$ produced in $e^+e^- \to \psi(3770) \to D^0\overline{D}^0$, though the analysis presented here relies on D^0 mesons from D^{*+} meson decays in e^+e^- continuum production at $\sqrt{s} \approx 10.58$ GeV. This is the first analysis of the resonant substructures of $D^0 \to K^+K^-\pi^0$ and their interference. The relevant published individual branching ratios (BR) are $BR(D^0 \to K^+K^-\pi^0) = (0.13 \pm 0.04)\%$, $BR(D^0 \to K^{*+}K^-) = (0.37 \pm 0.08)\%$, $BR(D^0 \to K^{*-}K^+) = (0.20 \pm 0.11)\%$, and $BR(D^0 \to \phi\pi^0) = (0.076 \pm 0.005)\%$ [4–8].

Three-body decays of D mesons are expected to be dominated by resonant two body decays [9–13] and the well established Dalitz plot analysis technique [14] can be used to explore their relative amplitudes and phases. The CLEO collaboration has published Dalitz plot analyses for several three-body D^0 decays over the past few years [15–20] and the work described here closely follows the methods developed in these previous analyses.

This analysis uses an integrated luminosity of 9.0 fb^{-1} of e^+e^- collisions at $\sqrt{s} \approx 10.58$ GeV provided by the Cornell Electron Storage Ring (CESR). The data were collected with the CLEO III detector [21–23]. To suppress backgrounds and to tag the flavor $D^0(\overline{D}^0)$, the D^0 mesons are reconstructed in the decay sequence $D^{*+} \to \pi_s^+ D^0$, where the sign of the slow pion $\pi_s^+(\pi_s^-)$ tags the flavor of the $D^0(\overline{D}^0)$ at the time of its production.

The detected charged particle tracks must reconstruct to within 5 cm of the interaction point along the beam pipe and within 5 mm perpendicular to the beam pipe (the typical beam spot is 300 μm in the horizontal dimension, 100 μm in the vertical dimension, and 10 mm in the longitudinal dimension). The cosine of the angle between a track and the nominal beam axis must be between -0.9 and 0.9 in order to assure that the particle is in the fiducial volume of the detector. The π_s candidates are required to have momenta $150 \le p_{\pi_s} \le 500$ MeV$/c$, and kaon candidates are required to have momenta $200 \le p_K \le 5000$ MeV$/c$. Candidate kaon tracks that have momenta greater than or equal to 500 MeV$/c$ are selected based on information from the Ring Imaging Cherenkov (RICH) detector [24] if at least four photons associated with the track are detected. The pattern of the Cherenkov photon hits in the RICH detector is fit to both a kaon and a pion hypothesis, each with its own likelihood $\mathcal{L}_K$ and $\mathcal{L}_\pi$. We require $(-2\ln\mathcal{L}_K) - (-2\ln\mathcal{L}_\pi) < 0$ for a kaon candidate to be accepted. Candidate kaon tracks without RICH information or with momentum below 500 MeV$/c$ are required to have specific energy loss in the drift chamber within 2.5 standard deviations of that expected for a true kaon.

The π^0 candidates are reconstructed from all pairs of electromagnetic showers that are not associated with charged tracks. To reduce the number of fake π^0s from random shower combinations, we require that each shower have an energy greater than 100 MeV and be in the barrel region of the detector. The two photon invariant mass is required to be within 2.5 standard deviations of the known π^0 mass. To improve the resolution on the π^0 three-

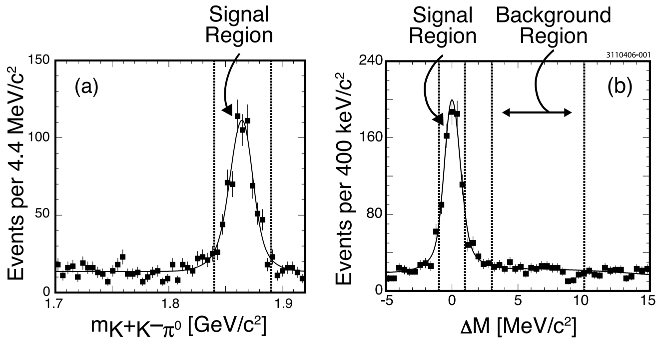

FIG. 1: Distribution of (a) $m_{K^+K^-\pi^0}$ for $|\Delta M| < 1$ MeV$/c^2$ and (b) ΔM for $1.84 < m_{K^+K^-\pi^0} < 1.89$ GeV$/c^2$ after passing all other selection criteria discussed in the text. The solid curves show the results of fits to the $m_{K^+K^-\pi^0}$ and ΔM distributions, respectively. The vertical lines in (a) and the left-most set of vertical lines in (b) denote the signal region. The right-most set of vertical lines in figure (b) denote the ΔM sideband used for estimation of the background shape.

momentum, the $\gamma\gamma$ invariant mass is constrained to the known π^0 mass.

We reconstruct the decay chain $D^{*+} \to \pi_s^+ D^0$, $D^0 \to K^+K^-\pi^0$ with the requirement that the D^{*+} momentum be at least as large as one-half of its maximum allowed value in order to suppress large combinatoric backgrounds from B-meson decays. The D^0 candidate invariant mass $m_{K^+K^-\pi^0}$ and invariant $D^{*+} - D^0$ mass difference $\Delta M \equiv m_{K^+K^-\pi^0\pi_s^+} - m_{K^+K^-\pi^0} - (m_{D^{*+}} - m_{D^0})$ are calculated for each candidate, where $m_{D^{*+}}$ and m_{D^0} are taken from Ref. [4]. The distributions of $m_{K^+K^-\pi^0}$ and ΔM are shown in Fig. 1. We fit each of the distributions to the sum of two bifurcated Gaussians plus a background shape which is constant (for $m_{K^+K^-\pi^0}$) or parabolic (for ΔM). We find an average signal fraction of $(81.8 \pm 6.3 \pm 2.8)\%$, where the systematic error is half of the difference between the signal fraction from the fits to $m_{K^+K^-\pi^0}$ and ΔM. We select a signal region defined by $1.84 < m_{K^+K^-\pi^0} < 1.89$ GeV$/c^2$ and $|\Delta M| < 1$ MeV$/c^2$ which contains 735 $D^0 \to K^+K^-\pi^0$ candidates.

We expect CP violation in D decay to be negligible and assume the amplitudes for $D^0 \to K^{*-}K^+$ and $D^0 \to K^{*+}K^-$ are equal to the amplitudes for charge-conjugated modes $\overline{D}^0 \to K^{*+}K^-$ and $\overline{D}^0 \to K^{*-}K^+$, respectively. This allows us to double our statistics in a single Dalitz plot by combining flavor-tagged $D^0 \to K^+K^-\pi^0$ and $\overline{D}^0 \to K^+K^-\pi^0$ candidates and choosing the $m^2_{K^-\pi^0}$ variable for one to be the $m^2_{K^+\pi^0}$ variable for the other (and vice versa). The inclusion of charge conjugate modes is implied throughout this paper.

Figure 2(a) shows the Dalitz plot distribution for the $D^0 \to K^+K^-\pi^0$ candidates. The enhanced bands perpendicular to the $m^2_{K^-\pi^0}$ and $m^2_{K^+\pi^0}$ axes at an invariant mass-squared of $m^2_{K\pi} \approx 0.8$ GeV$^2/c^4$ correspond to $K^*(892)^-$ and $K^*(892)^+$ resonances, respectively. The $\phi(1020)$ can be seen as a diagonal band along the upper right edge of the plot. The vector nature of these resonances is evident from the depleted region in the middle of each band. The nearly missing bottom lobe of the $K^*(892)^-$ band and the enhanced left lobe of the $K^*(892)^+$ band show that these resonances are interfering with opposite phases with the S-wave amplitude under these resonances.

We parameterize the $D^0 \to K^+K^-\pi^0$ Dalitz plot following the methodology described in [15–20]. We express the amplitude for D^0 to the $j^{\rm th}$ quasi-two-body state as $a_j e^{i\delta_j}\mathcal{B}_j^{(k)}$, where a_j is real and positive and $\mathcal{B}_j^{(k)}$ is the Breit-Wigner amplitude for resonance j with spin k described in Ref. [15]. Our sign convention implies that $\delta_D \equiv \delta_{K^{*-}K^+} - \delta_{K^{*+}K^-} = 0°$ (180°)

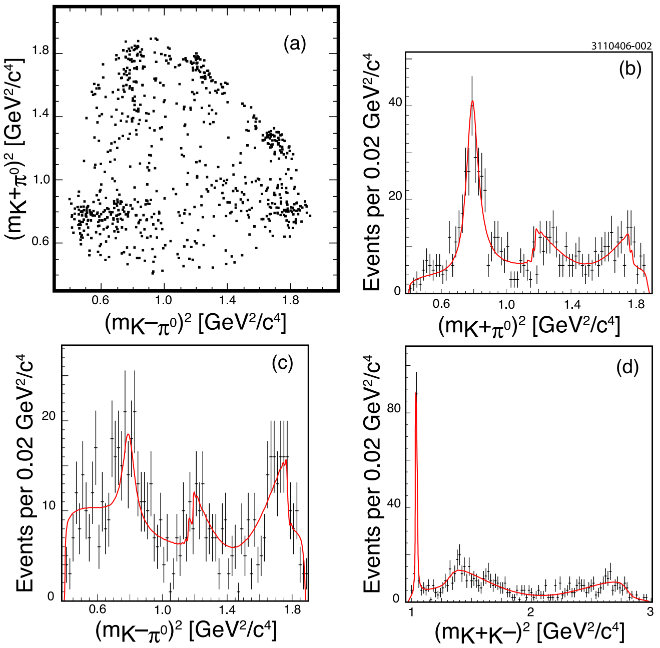

FIG. 2: (a) The Dalitz plot distribution for $D^0 \to K^+K^-\pi^0$ candidates. (b)-(d) Projections onto the $m^2_{K^+\pi^0}$, $m^2_{K^-\pi^0}$, and $m^2_{K^+K^-}$ axes of the results of Fit A showing both the fit (curve) and the binned data sample. The curves of Fit B projections are indistinguishable from those of Fit A.

indicates maximal destructive (constructive) interference between the K^* amplitudes. We consider thirteen resonant components (see Table I) as well as a uniform non-resonant contribution. Dalitz plot analyses are only sensitive to relative phases and amplitudes, hence we may arbitrarily define the amplitude and phase for one of the two-body decay modes. The mode with the largest rate, $K^{*+}K^-$, is assigned an amplitude $a_{K^{*+}K^-} = 1$ and phase $\delta_{K^{*+}K^-} = 0°$.

The efficiency for the selection requirements described above is not expected to be uniform across the Dalitz plot because of the momentum dependent reconstruction algorithms near the edge of phase space. To study these variations, we produce Monte Carlo generated $D^{*+} \to \pi_s^+ D^0$, $D^0 \to K^+K^-\pi^0$ events (based on GEANT3 [25]) which uniformly populate the allowed phase space and pass them through our event processing algorithms. We observe a modest and smooth dependence of reconstruction efficiency on Dalitz plot position and fit this to a two dimensional cubic polynomial in $(m^2_{K^+\pi^0},\ m^2_{K^+K^-})$. The average reconstruction efficiency for the decay chain $D^{*+} \to \pi_s^+ D^0$, $D^0 \to K^+K^-\pi^0$ in our signal region is found to be $(5.8 \pm 0.1)\%$.

Figure 1 shows that the background is significant. To construct a model of the background shape, we consider events in the data sideband $3 < \Delta M < 10$ MeV/c^2 within the $m_{K^+K^-\pi^0}$ signal region defined above, as shown in Fig. 1(b). There are 384 events in this selection, about three times the amount of background we estimate in the signal region. The background is dominated by random combinations of unrelated tracks and showers. Although the background includes $K^{*\pm}$ and ϕ mesons combined with random tracks and/or showers, these events will not interfere with each other or with resonances in the signal. The background shape is well fitted by a two dimensional cubic polynomial in $(m^2_{K^+\pi^0},\ m^2_{K^+K^-})$ with non-interfering terms that represent $K^{*\pm}$ and ϕ mesons.

Resonance r	m_r (GeV/c^2)	Γ_r (GeV/c^2)
$K^*(892)^\pm$	0.8917	0.0508
$\phi(1020)$	1.0190	0.0043
non-resonant	flat	flat
$a_0(980)$	0.9910	0.0690
$f_0(1370)$	1.3500	0.2650
$K_0(1430)^\pm$	1.4120	0.2940
$K_2(1430)^\pm$	1.4260	0.0985
$f_0(1500)$	1.5070	0.1090
$f'_2(1525)$	1.5250	0.0730
$\kappa^\pm$	0.8780	0.4990

TABLE I: The masses and widths of resonances r considered in this analysis [4, 26–28].

	Amplitude	Phase (°)	Fit Fraction (%)
Fit A			
SL = 18.6%			
K^{*+}	1 (fixed)	0 (fixed)	46.1 ± 3.1
K^{*-}	$0.52 \pm 0.05 \pm 0.04$	$332 \pm 8 \pm 11$	12.3 ± 2.2
ϕ	0.64 ± 0.04	326 ± 9	14.9 ± 1.6
NR	5.62 ± 0.45	220 ± 5	36.0 ± 3.7
Fit B			
SL = 17.2%			
K^{*+}	1 (fixed)	0 (fixed)	48.1 ± 4.5
K^{*-}	0.52 ± 0.05	313 ± 9	12.9 ± 2.6
ϕ	0.65 ± 0.05	334 ± 12	16.1 ± 1.9
κ^+	1.78 ± 0.43	109 ± 17	12.6 ± 5.8
κ^-	1.60 ± 0.29	128 ± 17	11.1 ± 4.7

TABLE II: Dalitz plot fit results. The model for Fit A includes $K^{*\pm}$, ϕ, and a non-resonant contribution. The model for Fit B includes $K^{*\pm}$, ϕ, and $\kappa^\pm$. A significance level (SL), calculated by the method of Ref. [29], is shown for each fit.

We use the background and efficiency parameterizations in our Dalitz plot fit to the data. Our results are presented in Table II. Fit A includes the $K^*(892)^\pm$ and $\phi(1020)$ resonances plus an interfering non-resonant (NR) component and is shown in Fig. 2(b)-(d). For each entry in Table II, the first error shown is statistical. Systematic errors are also shown for the K^* submodes, since those are the results that ultimately contribute to the phase difference and relative amplitudes this analysis seeks to measure. The determination of these systematic errors is discussed below.

Since it is difficult to distinguish a simple NR contribution from a broad S-wave component, we investigated the effect of replacing the NR component of Fit A with broad S-wave $\kappa^\pm \to K^\pm\pi^0$ resonances parameterized using Breit-Wigner amplitudes [26]. The result of this substitution is shown as Fit B in Table II. Both Fit A and Fit B have good significance levels, and the projections of Fit A and Fit B are indistinguishable, hence we have no reason to prefer one fit over the other. Significance levels are calculated by the method of Ref. [29].

We tested other combinations of broad amplitudes as possible replacements to the simple non-resonant component, including one fit with $K_0(1430)^\pm \to K^\pm\pi^0$ and $\kappa^\pm \to K^\pm\pi^0$ and another fit with a NR component combined with $K_0(1430)^\pm$. We did not find that either of these fits were preferable to Fit A or Fit B, although we do include these results when determining our model systematic error. We did not find significant evidence for any of the other resonances listed in Table I. A fit which included only $K^{*\pm}$ and ϕ contributions (without a NR component) was significantly worse than Fit A.

Since the choice of normalization, phase convention, and amplitude formalism may not always be identical for different experiments, fit fractions are reported in addition to amplitudes. The fit fraction is defined as the integral of a single component (resonant or non-resonant) over the Dalitz plot, divided by the integral of the coherent sum of all components over the Dalitz plot [15]. The sum of the fit fractions for all components will not necessarily be unity because of interference in the coherent sum.

We use the full covariance matrix from Fit A and Fit B to determine the statistical errors on the fit fractions and to properly include the correlated components of the uncertainty on the amplitudes and phases. After each fit, the covariance matrix and final parameter values are used to generate a large number of sample parameter sets. Fit fractions are calculated as described above for each set of parameters, and the Gaussian widths of these distributions represent the statistical errors on the nominal fit fractions.

The strong phase difference δ_D and relative amplitude r_D are defined as follows:

$$r_D e^{i\delta_D} = \frac{a_{K^{*-}K^+}}{a_{K^{*+}K^-}}\, e^{i(\delta_{K^{*-}K^+} - \delta_{K^{*+}K^-})}, \tag{1}$$

where r_D in Eq. (1) is defined as real and positive. The strong phase difference is equivalent to the overall phase difference due to our assumption that CP violation in D decays is negligible. With this definition we can simply read our nominal results from Fit A of Table II:

$$\delta_D = 332^\circ \pm 8^\circ \pm 11^\circ, \quad r_D = 0.52 \pm 0.05 \pm 0.04.$$

We consider systematic errors from experimental sources and from the decay model separately. Contributions to the *experimental* systematic uncertainties arise from our models of the background, the efficiency, the signal fraction, and the event selection. Our general procedure is to change some aspect of the analysis and interpret the change in the values of the amplitude ratio r_D and phase difference δ_D as an estimate of the associated systematic uncertainty. In Fit A, we fix the coefficients of the background parameterization to the values found in our fit to the sideband region as described above. To estimate the systematic uncertainty on this background shape, we perform a fit where these coefficients are allowed to float constrained by the covariance matrix of the background fit. A similar method is used to determine the systematic uncertainty for the efficiency shape. We change selection criteria in the analysis to test whether our Monte Carlo simulation properly models the efficiency. We vary the minimum π^0 daughter energy, the cuts on $m_{K^+K^-\pi^0}$ and ΔM, the D^{*+} minimum momentum fraction, the $m(\gamma\gamma) - m(\pi^0)$ requirement, and the RICH and specific energy criteria. We allow the width of the $\phi(1020)$ to float to accommodate detector resolution effects. We performed partial fits of the Dalitz plot excluding regions not close to the $K^*(892)$ bands, and we changed the invariant mass-squared variables in our fits from $(m^2_{K^+\pi^0},\ m^2_{K^+K^-})$ to $(m^2_{K^-\pi^0},\ m^2_{K^+\pi^0})$. The largest experimental systematic uncertainties are $\pm 8^\circ$ for δ_D when allowing the background parameters to float, and ± 0.05 for r_D when allowing the efficiency parameters to float, as described above.

The *model* systematic error arises from uncertainty in the choice of resonances used to fit the Dalitz plot. We fit the data to many models that incorporate various combinations of the resonances listed in the lower part of Table I in addition to the $K^*(892)^\pm$ and $\phi(1020)$. We allow our κ mass and width to float in a separate fit, finding the preferred values to be $m_\kappa = (855 \pm 15)$ MeV and $\Gamma_\kappa = (251 \pm 48)$ MeV. The significance level for the fit where the κ mass and width float is 16.2%. The floating κ mass is consistent with Ref. [26], but the floating κ width is smaller by about two standard deviations. We use our measured error and the error from Ref. [26] on Γ_κ to calculate the deviation.

We determine the total experimental and model systematic uncertainties separately. We take the square root of the sample variance of the amplitudes and phases from the nominal result compared to the results in the series of fits described above as a measure of the systematic uncertainty. We find $\pm 2.9^\circ$(exp.) $\pm$ 10.6°(model) for δ_D and ± 0.016(exp.) $\pm$ 0.038(model) for r_D. Adding systematic errors in this way results in a model systematic error for δ_D that is less than the difference in δ_D when comparing Fit A to Fit B. We add the experimental and model systematic uncertainty in quadrature to obtain the total systematic uncertainty reported in Table II.

Our systematic error is dominated by the model dependence, and the largest deviations from the nominal fit were observed in the series of fits where we replaced the non-resonant contribution with the $\kappa^\pm$. If fits including a $\kappa^\pm$ resonance are removed from consideration, then the systematic errors on δ_D and r_D decrease from $\pm 11^\circ$ and ± 0.04 to $\pm 8^\circ$ and ± 0.03, respectively, and the remaining systematic uncertainty is dominated by fits including the $K_0(1430)^\pm$.

As a cross-check, we estimate the branching ratio of $D^0 \to K^+K^-\pi^0$ from our data and compare it to the published value. Branching ratio measurements are not the focus of this analysis, so systematic errors have not been investigated. Based on our $m_{K^+K^-\pi^0}$ fit, we have a total of 627 ± 30 signal events. We may estimate the total number of D^0s expected from continuum D^{*+}s in our data sample, based on the integral cross-section for continuum D^{*+} production near $\sqrt{s} = 10.6$ GeV [30]: $\sigma(e^+e^- \to D^{*+}X) = (583 \pm 8 \pm 33 \pm 14)$ pb, where the fourth error stems from external branching fraction uncertainties. From this information and $BR(D^{*+} \to \pi_s^+ D^0)$ [4], we estimate $BR(D^0 \to K^+K^-\pi^0) = (0.30 \pm 0.02)\%$, which is significantly higher than the previous measurement [4, 5]. Combining our fit fractions with known values for $BR(K^{*\pm} \to K^\pm\pi^0)$ and $BR(\phi \to K^+K^-)$ [4], we also estimate branching ratios of the resonant decay modes. We find $BR(D^0 \to K^{*+}K^-) = (0.38 \pm 0.04)\%$, $BR(D^0 \to K^{*-}K^+) = (0.10 \pm 0.02)\%$, and $BR(D^0 \to \phi\pi^0) = (0.084 \pm 0.012)\%$. These branching ratios are consistent with published measurements [4, 6–8].

U-spin symmetry [31] predicts the following for D^0 decays to a pseudoscalar meson and a vector meson:

$$\mathcal{A}(D^0 \to \pi^+\rho^-) = -\mathcal{A}(D^0 \to K^+K^{*-}) \tag{2}$$

and

$$\mathcal{A}(D^0 \to \pi^-\rho^+) = -\mathcal{A}(D^0 \to K^-K^{*+}), \tag{3}$$

where $\mathcal{A}$ is the respective dimensionless invariant amplitude for each decay. Dividing Eq. (2)

by Eq. (3), and assuming that $\mathcal{A}(K^{*+} \to K^+\pi^0) = \mathcal{A}(K^{*-} \to K^-\pi^0)$, gives:

$$\frac{\mathcal{A}(D^0 \to \pi^+\rho^-)}{\mathcal{A}(D^0 \to \pi^-\rho^+)} = \frac{a_{K^{*-}K^+}}{a_{K^{*+}K^-}}\; e^{i(\delta_{K^{*-}K^+} - \delta_{K^{*+}K^-})}. \tag{4}$$

Assuming a phase convention such that a phase difference of 0° indicates maximal destructive interference between ρ^- and ρ^+, and assuming $\mathcal{A}(\rho^+ \to \pi^+\pi^0) = \mathcal{A}(\rho^- \to \pi^-\pi^0)$, we can use the recently published results of a Dalitz plot analysis of $D^0 \to \pi^+\pi^-\pi^0$ [16] to evaluate the left hand side of Eq. (4):

$$(0.65 \pm 0.03 \pm 0.02)e^{i(356^\circ \pm 3^\circ \pm 2^\circ)}$$

which may be compared to the right hand side of Eq. (4) which comes from this analysis:

$$(0.52 \pm 0.05 \pm 0.04)e^{i(332^\circ \pm 8^\circ \pm 11^\circ)}.$$

In conclusion, we have examined the resonant substructure of the decay $D^0 \to K^+K^-\pi^0$ using the Dalitz plot analysis technique. We observe resonant $K^{*+}K^-$, $K^{*-}K^+$, and $\phi\pi^0$ contributions. We also observe a significant S-wave modeled as a $\kappa^\pm K^\mp$ or a non-resonant contribution. We determine $\delta_D = 332^\circ \pm 8^\circ \pm 11^\circ$ and $r_D = 0.52 \pm 0.05 \pm 0.04$.

We gratefully acknowledge the effort of the CESR staff in providing us with excellent luminosity and running conditions. D. Cronin-Hennessy and A. Ryd thank the A.P. Sloan Foundation. This work was supported by the National Science Foundation, the U.S. Department of Energy, and the Natural Sciences and Engineering Research Council of Canada.

---

[1] J. Charles *et al.* [CKMfitter Group], Eur. Phys. J. C **41**, 1-131 (2005). Updated results and plots available at: http://ckmfitter.in2p3.fr
[2] Y. Grossman, Z. Ligeti, and A. Soffer, Phys. Rev. D **67**, 071301 (2003).
[3] J. L. Rosner and D. A. Suprun, Phys. Rev. D **68**, 054010 (2003).
[4] S. Eidelman *et al.* [Particle Data Group], Phys. Lett. B **592**, 1 (2004).
[5] D. M. Asner *et al.* [CLEO Collaboration], Phys. Rev. D **54**, 4211 (1996).
[6] R. Ammar *et al.* [CLEO Collaboration], Phys. Rev. D **44**, 3383 (1991).
[7] H. Albrecht *et al.* [ARGUS Collaboration], Z. Phys. C **46**, 9 (1990).
[8] O. Tajima *et al.* [Belle Collaboration], Phys. Rev. Lett. **92**, 101803 (2004).
[9] M. Bauer, B. Stech, and M. Wirbel, Z. Phys. C **34**, 103 (1987).
[10] P. F. Bedaque, A. K. Das, and V. S. Mathur, Phys. Rev. D **49**, 269 (1994).
[11] L. L. Chau and H. Y. Cheng, Phys. Rev. D **36**, 137 (1987).
[12] K. Terasaki, Int. J. Mod. Phys. A **10**, 3207 (1995).
[13] F. Buccella *et al.*, Phys. Lett. B **379**, 249 (1996).
[14] D. Asner, "Dalitz Plot Analysis Formalism Review," on page 664 of Ref. [4].
[15] S. Kopp *et al.* [CLEO Collaboration], Phys. Rev. D **63**, 092001 (2001).
[16] D. Cronin-Hennessy *et al.* [CLEO Collaboration], Phys. Rev. D **72**, 031102 (2005).
[17] H. Muramatsu *et al.* [CLEO Collaboration], Phys. Rev. Lett. **89**, 251802 (2002).
[18] D. M. Asner *et al.* [CLEO Collaboration], Phys. Rev. D **70**, 091101 (2004).
[19] P. Rubin *et al.* [CLEO Collaboration], Phys. Rev. Lett. **93**, 111801 (2004).
[20] D. M. Asner *et al.* [CLEO Collaboration], Phys. Rev. D **72**, 012001 (2005).

[21] Y. Kubota *et al.* [CLEO Collaboration], Nucl. Instrum. Methods Phys. Res., Sect. A **320**, 66 (1992).
[22] T. S. Hill, Nucl. Instrum. Methods Phys. Res., Sect. A **418**, 32 (1998).
[23] G. Viehhauser, Nucl. Instrum. Methods Phys. Res., Sect. A **462**, 146 (2001).
[24] M. Artuso *et al.*, Nucl. Instrum. Meth. Phys. Res., Sect A **554**, 147 (2005).
[25] R. Brun *et al.*, Geant 3.21, CERN Program Library Long Writeup W5013 (1993), unpublished.
[26] M. Ablikim *et al.* [BES Collaboration], Phys. Lett. B **633**, 681 (2006).
[27] S. Teige *et al.* [E852 Collaboration], Phys. Rev. D **59**, 012001 (1998).
[28] M. Ablikim *et al.* [BES Collaboration], Phys. Lett. B **607**, 243 (2005).
[29] H. Albrecht *et al.* [ARGUS Collaboration], Phys. Lett. B **308**, 435 (1993).
[30] M. Artuso *et al.* [CLEO Collaboration], Phys. Rev. D **70**, 112001 (2004).
[31] C. Chiang, Z. Luo, and J. L. Rosner, Phys. Rev. D **67**, 014001 (2003).